Journal Pre-proof

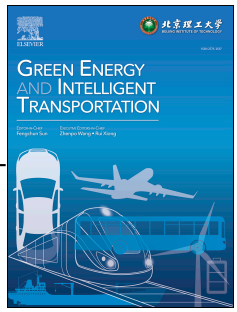

A Nonlinear Galloping-Driven Triboelectric-Electromagnetic Hybrid Generator for Low-Speed Wind Energy Harvesting

Xilong Kang, Pengbo Li, Yawei Wang, Renyun Zhang, Yizhou Li, Yupei Jian, Quanke Su, Guobiao Hu, Junlei Wang

PII: S2773-1537(25)00113-6

DOI: https://doi.org/10.1016/j.geits.2025.100363

Reference: GEITS 100363

To appear in: *Green Energy and Intelligent Transportation*

Received Date: 20 August 2025

Revised Date: 10 September 2025

Accepted Date: 15 September 2025

Please cite this article as: Kang X, Li P, Wang Y, Zhang R, Li Y, Jian Y, Su Q, Hu G, Wang J, A Nonlinear Galloping-Driven Triboelectric-Electromagnetic Hybrid Generator for Low-Speed Wind Energy Harvesting, *Green Energy and Intelligent Transportation*, https://doi.org/10.1016/j.geits.2025.100363.

A Nonlinear Galloping-Driven Triboelectric-Electromagnetic Hybrid Generator for Low-Speed Wind Energy Harvesting

Xilong Kang[1,#], Pengbo Li[1,#], Yawei Wang[2], Renyun Zhang[3], Yizhou Li[2], Yupei Jian[4], Quanke Su[5], Guobiao Hu[2,*], Junlei Wang[1,*]

[1.] *School of Mechanical and Power Engineering, Zhengzhou University, Zhengzhou 450001, China;*
[2.] *Thrust of the Internet of Things, The Hong Kong University of Science and Technology (Guangzhou), Guangzhou 511400, China*
[3.] *Department of Natural Sciences, Mid Sweden University, Holmgatan 10, SE85170 Sundsvall, Sweden.*
[4.] *School of Electrical Engineering, Southwest Jiaotong University, Chengdu, 610031, China*
[5.] *Thrust of Intelligent Transportation, The Hong Kong University of Science and Technology (Guangzhou)*, *Nansha, Guangzhou 511400, China*

[#] *These authors contribute equally to this paper.*
**Correspondence:* guobiaohu@hkust-gz.edu.cn *(G.H.);* jlwang@zzu.edu.cn *(J.W.)*

Resources availability

Materials availability

This study did not generate new, unique reagents.

Data and code availability

The data and code that support the conclusions of this study are also available from the lead contact upon reasonable request.

Supporting Information

Author contributions

X.K., P.L., and J.W. conceived the idea. X.K., G.H. and J.W. secured the funding. X.K. and P.L. designed the experiment, conducted the test and measurements, collected the data, and drafted the original manuscript. X.K., P.L., and Y.W. prepared the figures. Y.W. and Y.L. designed and developed the circuit boards. R.Z., Y.J., G.H., and Q.S. polished the manuscript. G.H. and J.W. supervised and guided the project.

Acknowledgments

This work was supported by the National Natural Science Foundation of China (Grant Nos. 52277227 and 52305135), the Key Scientific and Technological Project of Henan Province (Grant No. 252102241025), and the Guangdong Provincial Project (Grant No. 2023QN10L545).

System Design

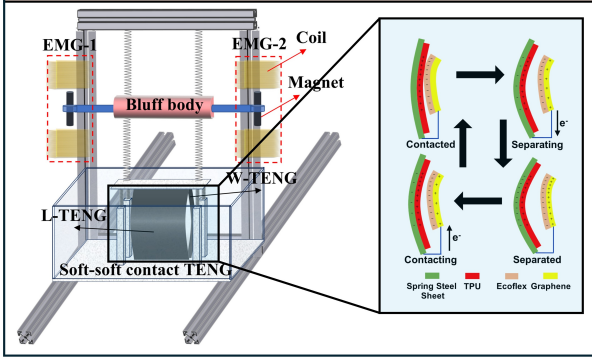

Optimization Strategy

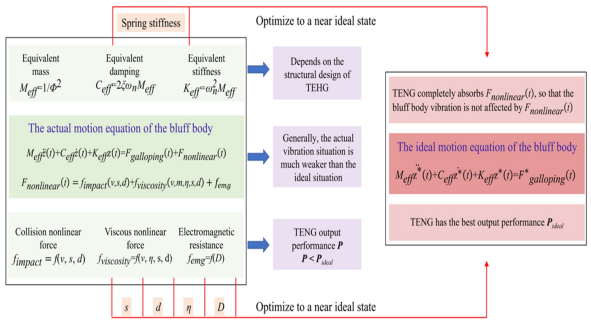

Application Demonstration

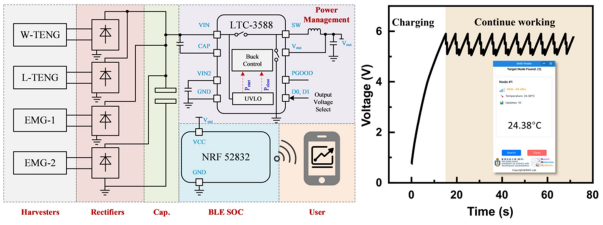

Performance Evaluation

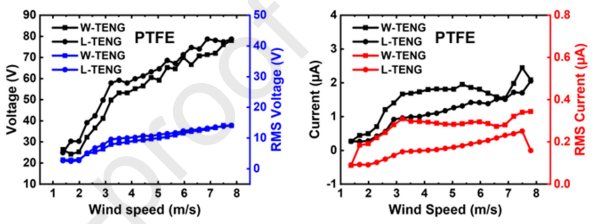

A Nonlinear Galloping-Driven Triboelectric-Electromagnetic Hybrid Generator for Low-Speed Wind Energy Harvesting

***

Abstract:

Triboelectric nanogenerators (TENGs) have emerged as a prominent technology for self-powered systems due to their remarkable outputs, low cost, and customizable structural designs. When integrated with flow-induced vibration (FIV), TENGs present a promising potential for harvesting low-speed wind energy. This study introduces a novel nonlinear galloping-driven triboelectric-electromagnetic hybrid generator (NG-TEHG) that can adapt to a wide range of wind speeds. We provide a comprehensive quantitative analysis of the nonlinear coupling effects between the TENG and bluff body galloping dynamics, revealing their impacts on the energy harvesting performance of the NG-TEHG. Our experimental results demonstrate that the NG-TEHG operates effectively within a wind speed range of 2.29–7.80 m/s, delivering a peak power of 10 mW and an RMS power of 3.34 mW at a wind speed of 4.74 m/s. This achieved power is sufficient to continuously drive a wireless temperature sensing node, showcasing the NG-TEHG's potential for practical applications. The hybrid system introduced in this study not only extends the range of wind energy harvesting but also provides a novel approach to galloping-based energy harvesting technologies.

Keywords: triboelectric nanogenerator (TENG); flow-induced vibration; galloping; hybrid energy harvesting; nonlinear coupling dynamics

1. Introduction

Low-speed wind energy is an abundant yet underutilized form of clean energy that holds promise for sustainable power generation. Triboelectric nanogenerators (TENGs), known for their excellent performance at low frequencies, strong scalability, and low cost, offer an ideal solution for harvesting such energy to build self-powered wireless sensing systems.[1-3] Notably, low-speed wind energy is typically treated as a steady fluid, and when such a fluid flows over a structure, the fluid-structure interaction (FSI) may induce self-excited vibration. This phenomenon, referred to as flow-induced vibration (FIV), can be leveraged as an efficient mechanism for mechanical-to-electrical energy conversion.[4] TENGs that operate based on the FIV principle, referred to as FIV-TENGs, often exhibit stable and superior performance and have thus been widely employed for harvesting flow-kinetic energy from wind, water, and other fluid environments.[5]

FIVs can be further classified into flutter,[6] vortex-induced vibration (VIV),[7] and galloping,[8] each exhibiting distinct characteristics suitable for different environments. These features enable the design of tailored TENGs to operate under low wind speeds, adapt to a wide range of wind speeds, and accommodate compact configurations.[9] Galloping is a self-excited vibration phenomenon driven by aerodynamic forces that introduce negative damping. It typically occurs in structures with complex, irregular, non-streamlined cross-sections, such as square, rectangular, and right-angled profiles. Galloping enables continuous energy harvesting from ambient airflow, making it well-suited for triboelectric nanogenerators (TENGs).[10,11] As an early demonstration of FIV-driven TENGs, the flag-shaped design stands out as a representative prototype.[12,13] Building on this concept, Yu *et al.*[14] designed an elastically assisted TENG with self-charge excitation, in which the flutter film was encapsulated with aluminum foil to mitigate environmental interference. Son *et al.*[15] proposed a dual-flagpole TENG with grooved structures to enable bidirectional wind energy harvesting. Yue *et al.*[16] developed a "mortise-and-tenon" micro-structured flutter film, achieving a power density of 455.932 mW/cm² and an output voltage of 7.5 kV at a wind speed of 7.9 m/s

using an array of flag-shaped TENGs. Furthermore, the output performance of flag-shaped TENGs can be enhanced by placing a bluff body upstream to reinforce the downstream flow field.[17,18] Dong *et al*.[19] placed bluff bodies with different metasurfaces upstream of the flag-shaped TENG, resulting in enhanced power output and improved linearity in wind speed sensing. However, all these devices require the flutter films to be directly exposed to the atmosphere, leading to two critical durability challenges: (1) output degradation due to prolonged exposure to environmental stressors (humidity, temperature fluctuations, and airborne particulates), and (2) gradual mechanical failure (edge curling, wrinkling, and ultimately tearing) resulting from repetitive deformation and friction-induced polarization.

To address the above-mentioned challenges, numerous studies have explored the use of bluff body vibrations to drive TENGs in recent years. [20,21] Those designs are typically realized by either attaching a bluff body to the free end of a cantilever beam or springs, both forming elastically suspended oscillator systems. When stable fluid flows over the bluff body, fluid-structure interaction occurs.[22] Such systems allow for the integration of TENGs inside bluff bodies.[23] A widely adopted strategy utilizes rolling beads to build the TENG, where the rolling beads can effectively convert the bluff body's vibrational energy into electrical power. As an alternative approach, Guo *et al*.[24] installed a switch-shuttling TENG inside a cylindrical-hexagram bluff body and provided a self-powered water quality monitoring solution. However, this approach increases the bluff body's mass, which in turn alters its dynamics.[25] In addition, the inherent geometric constraints of bluff bodies may limit the design flexibility of the TENGs. This limitation can be circumvented by using non-invasive space integration strategies, with one simple and effective approach being the rigid attachment of TENGs to the exterior of the bluff body or the cantilever beam. For instance, Kim *et al*.[26] mounted a free-standing-sliding (FS) mode TENG and a contact-separation (CS) mode TENG on the top of a cylindrical bluff body. Zhang *et al*.[27] installed a CS-mode TENG near a cantilever beam, utilizing beam vibration to excite the device. However, this

setup inevitably leads to collision-induced damage, degrading the output performance of the TENG. An alternative and effective approach is to employ spring connections between the bluff body and the TENG.[28,29] Such elastically coupled systems demand synchronization between TENG's operation and the bluff body's vibration while being affected by intricate nonlinear factors.[30-32]

In this study, we present a high-performance triboelectric-electromagnetic hybrid generator driven by galloping (NG-TEHG), capable of harvesting wind energy across a tunable range. This study investigates the effects of the system stiffness, configuration geometry, and triboelectric material viscosity on the performance of the NG-TEHG. An interesting finding is that by changing the viscosity of the triboelectric material, the NG-TEHG achieves an adjustable wind energy harvesting range. The operational range of the NG-TEHG first increases and then locks into a safe region (2.29-7.80 m/s) following the bluff body's vibration. The peak and average power outputs of this NG-TEHG reach approximately 10 mW and 3.34 mW, indicating 2.14-fold and 18.55-fold improvements, respectively, compared to purely triboelectric and electromagnetic designs.[28] Due to its excellent performance, the NG-TEHG can power a wireless temperature sensor stably.

2. Structural Configuration and Optimization Strategy

Galloping is a common form of flow-induced vibration, typically characterized by periodic oscillations when the wind speed exceeds a critical threshold. The oscillation amplitude increases with increasing wind speed. This facilitates efficient wind energy harvesting across a wide wind speed range. Building on this unique property and aiming to enhance structural scalability, we propose an elastically attached bluff body-TENG configuration, as shown in **Fig. 1**(a). This configuration consists of a windward TENG (W-TENG) and a leeward TENG (L-TENG), with the details illustrated in **Fig. S1** in the Supplementary Information showing that the TENG unit in the NG-TEHG operates within an independent compartment. This design mitigates spatial constraints imposed by the bluff body's volume and prevents direct rigid impacts on it.[33] In addition, there

are two electromagnetic generators (EMGs) positioned on both sides of the bluff body to further enhance the output performance. The parameters of the EMGs are listed in **Tables S1** and **S2** in the Supplementary Information.

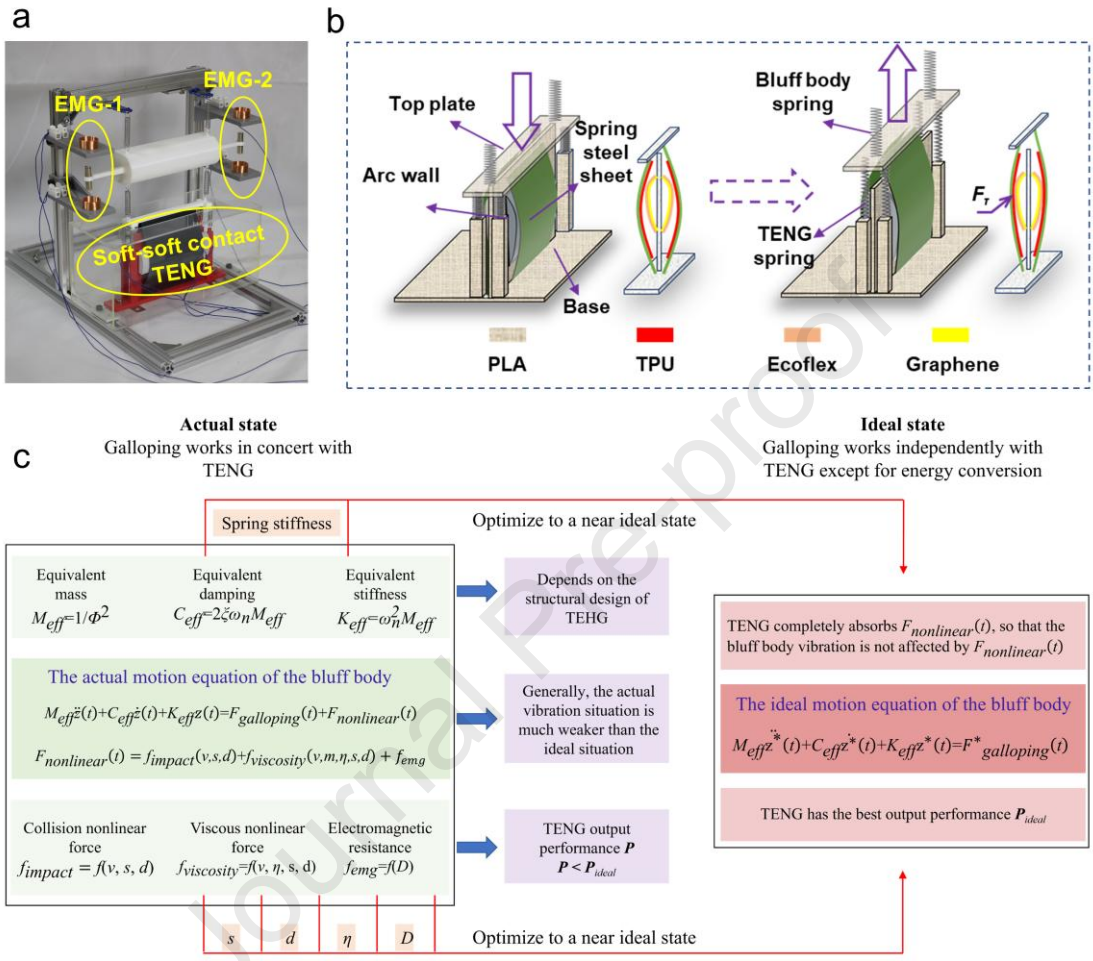

Fig.1 Structure design and optimization strategies of the NG-TEHG. (a) Photograph of the prototyped NG-TEHG, (b) Schematic diagram of the NG-TEHG, (c) Optimization strategy for the NG-TEHG.

The output performance of FIV-TENGs can be generally enhanced by optimizing the geometry of the bluff body, elastic suspension parameters, and triboelectric material properties.[34-36] Beyond these factors, for TENGs designed to operate within compartments elastically connected to the bluff body, the intricate coupling effects, particularly those arising from segmented springs and nonlinear damping during TENG operation, remain underexplored.[37,38] In this study, we systematically investigate these effects in the NG-TEHG, with detailed schematics of the TENG unit shown in **Fig. 1**(b). A 50 μm thick TPU film is coated on the spring steel sheet, serving as the positive

triboelectric material, and a high-performance flexible Ecoflex foam film is laminated onto the arc wall. The TENG unit functions as a spring-like element and is connected in series with the bluff body via real springs. This configuration enables the spring steel sheets to strike the arc wall in response to the bluff body's vibration, thereby activating TENG operation. As shown in **Fig. S2** in the Supplementary Information, contact between the spring steel sheet and arc wall induces charge transfer via the triboelectric effect, generating positive and negative charges on the TPU and Ecoflex foam films, respectively. Subsequently, during the separation process, electrons flow from the graphene electrode to the spring steel sheet, generating a current in the external circuit. When the separation distance reaches its maximum, the potential difference between the two electrodes also reaches its peak. As the spring steel sheet tends to reestablish contact with the arc wall, a reverse current is generated, and the potential difference between the two electrodes gradually reduces to zero. Once full contact is reestablished, the cycle is completed. This working cycle repeats continuously during the vibration of the bluff body, thus generating an alternating current that matches the vibration frequency. Through analysis of both bluff body geometry optimization and TENG material structure, it is concluded that during the operation of the NG-TEHG, the motion of the bluff body is controlled and influenced by three sets of nonlinear coupling forces: the aerodynamic force, the force from TENG unit, and the forces from two EMG units.

The nonlinear forces may alter the FIV mode, thereby affecting the efficiency of galloping. These nonlinear forces primarily include the impact force from spring steel sheets and viscous forces arising from the contact-separation process of the triboelectric material. These nonlinear effects can be changed by controlling four key parameters: the surface shape (s) of the arc wall, the initial distance (d) between the friction surfaces, the viscosity (η) of triboelectric material, and the initial gap (D) between the magnet and the coil. By systematically adjusting these parameters, the output performance of the NG-TEHG can be progressively optimized, and the specific optimization strategy

is shown in **Fig. 1**(c). Ideally, the TENG unit is expected to remain in resonance with the bluff body's galloping motion, thereby facilitating stable and efficient conversion of mechanical energy into electricity.

3. Results and Discussion

3.1. Structural tuning and dynamic enhancement of the NG-TEHG

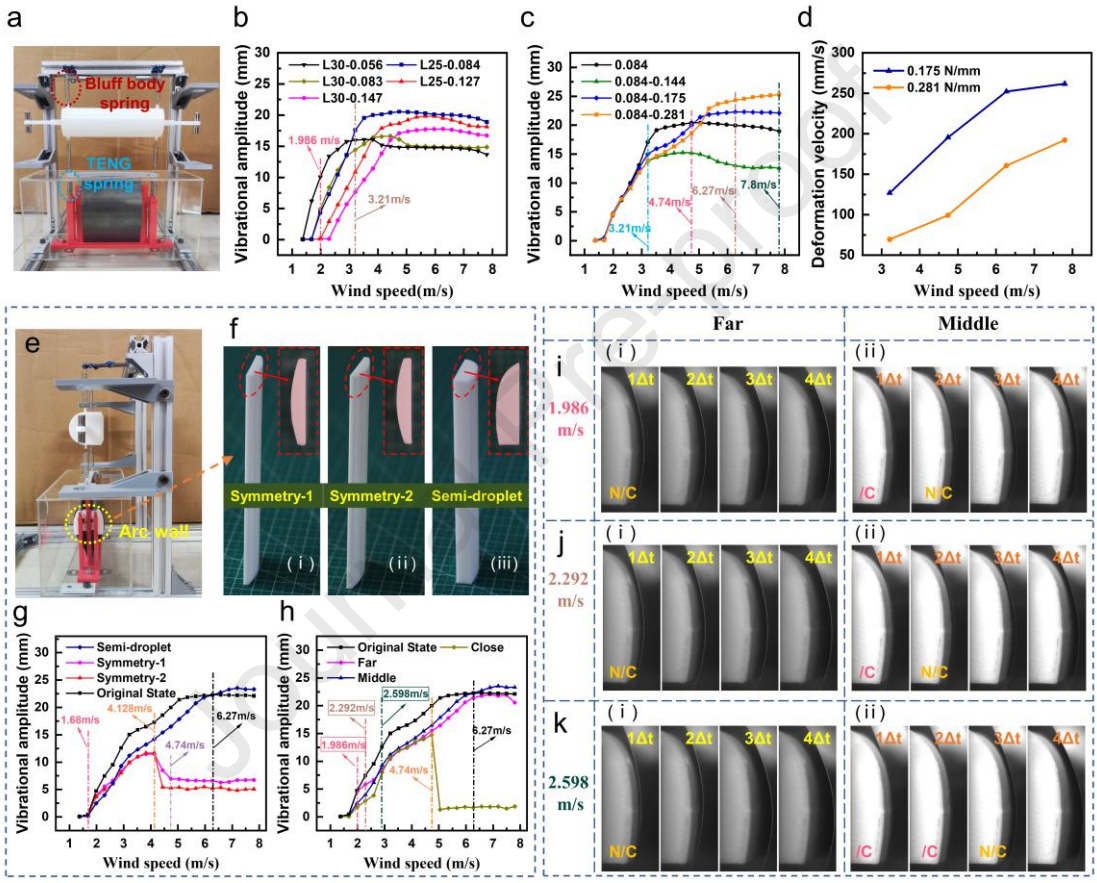

Fig.2 Structural optimization process of the NG-TEHG. (a) Front-view photograph of the NG-TEHG. Red dashed box: bluff body spring; blue dashed box: TENG spring. (b) Vibration amplitude responses of the bluff body suspended using different springs. Legend: L length - spring stiffness. (c) Vibration amplitude responses in response to variations in the TENG springs. Legend: bluff body spring stiffness-TENG spring stiffness. (d) Comparative analysis of TENG springs (0.175 N/mm vs. 0.281 N/mm). (e) Side-view photograph of the NG-TEHG. Yellow dashed box: arc wall. (f) Three arc wall configurations with different surface shapes. (g) Vibration amplitude responses of the three arc wall configurations. (h) Vibration responses under varying initial distances between the spring steel sheet and arc wall. (i-k) High-speed snapshots of spring steel sheet-wall interactions at wind speeds of 1.98 m/s, 2.29 m/s, and 2.59 m/s, showing collision (/C) and no collision (N/C) states at different initial distances.

The dynamics of any practical FIV systems are governed by their corresponding mechanical structures. In the proposed NG-TEHG, the equivalent mass and damping are primarily determined by the bluff body and the TENG unit, while the stiffness is governed by the springs. As shown in **Fig. 2**(a), the equivalent stiffness of the galloping system can be adjusted by changing the bluff body spring and TENG spring. Five types of bluff body springs and three types of TENG springs were tested to optimize galloping dynamics (see Supplementary **Table S3** for spring parameters). To evaluate the impact of different bluff body springs on galloping behavior, the bluff body was tested without connection to the TENG, and the obtained time-history responses are presented in **Fig. 2**(b). The results show that the NG-TEHG achieves optimal bluff body vibration when springs with a length of 25 mm and a stiffness of 0.084 N/mm are used, exhibiting both a lower onset wind speed and the ability to sustain large-amplitude vibrations at high wind speeds. It is worth noting that when the TENG was connected, the arc wall was not installed, thereby eliminating collision-induced nonlinear forces and viscous nonlinear forces. As shown in **Fig. 2**(c), among the three TENG springs tested, the spring with a stiffness of 0.144 N/mm performed the worst. The TENG spring, with a stiffness of 0.175 N/mm, produced weaker bluff body vibrations than the 0.281 N/mm spring at wind speeds below 5.05 m/s, but exhibited stronger vibrations at wind speeds above this threshold. For a more detailed comparison of the two TENG springs, we monitored the deformation of the spring steel sheets at four wind speeds: 3.21 m/s, 4.74 m/s, 6.27 m/s and 7.80 m/s (deformation images are provided in Supplementary **Fig. S3**). Using the operating frequency of the TENG at corresponding wind speeds, we calculated the deformation velocities of the spring steel sheets of the TENG springs, as shown in **Fig. 2**(d). These results indicate that the TENG spring with a stiffness of 0.175 N/mm more effectively converts the bluff body's vibration energy.

The surface shape (s) of the arc wall influences the nonlinear collision behavior when the spring steel sheet impacts it. As shown in **Fig. 2**(e, f), three configurations were designed for optimization: two symmetric profiles (Supplementary **Fig. S4**) and

one asymmetric semi-droplet shape. Symmetric surfaces are generally considered more compatible with the deformation of spring steel sheets, as they increase the contact area and thereby enhance nonlinear collision forces. However, experimental results show that both symmetric surfaces lead to a sharp decline in galloping vibration beyond 4.13 m/s, followed by a plateau, which suppresses the vibration under large wind speeds, as shown in **Fig. 2**(g). In contrast, the semi-droplet surface shape can sustain galloping, with amplitudes beyond 6.27 m/s surpassing those observed in the initial non-collision state. Therefore, this shape was adopted in the design of the arc wall.

In addition to the surface profile of the arc wall, it is also essential to optimize the initial distance (*d*) between the spring steel sheet and the arc wall. Three initial distances, namely, “Close”, “Middle”, and “Far”, were defined by adjusting the thickness of the arc wall. As shown in **Fig. 2**(h), when the initial distance is set to the closest position (Close), the galloping amplitude drops sharply at 4.74 m/s, significantly limiting the operational wind range of the NG-TEHG. When the initial distances are set to Middle and Far, the system can maintain galloping. At wind speeds above 2.59 m/s, the galloping amplitude at the Middle distance consistently exceeds that at the Far distance. Conversely, below 2.59 m/s, the galloping amplitude at the Middle distance remains lower than at the Far distance. **Fig. 2**(i, j, k) illustrates the contact timing sequence between the spring steel sheet and the arc wall at two initial distances under wind speeds of 1.98 m/s, 2.29 m/s, and 2.59 m/s. Earlier contact signifies a lower onset wind speed, which is favorable for wind energy harvesting. At wind speeds below 2.59 m/s, no collision (N/C) occurs at the Far distance, whereas at the Middle distance, collisions (/C) occur as early as 1.98 m/s. This suggests that a Middle initial distance between the spring steel sheet and the semi-droplet-shaped arc wall not only promotes TENG operation at lower wind speeds but also results in stronger galloping responses.

3.2. Material viscosity-controlled bandwidth tuning in the NG-TEHG

The optimized NG-TEHG ensures that the bluff body maintains galloping across

a wind speed range from 1.68 m/s to 7.80 m/s despite the presence of nonlinear collision effects between the spring steel sheet and the arc wall. Similar to the nonlinear collision effects, when a thermoplastic polyurethanes (TPU) film is attached to the spring steel sheet, and an Ecoflex foam film is attached to the arc wall surface, the TENG introduces nonlinear viscous effects due to material viscosity η during operation, thereby enabling the NG-TEHG to achieve a tunable operational wind speed range. To further explore the impact of material viscosity on the NG-TEHG, four sets of materials with different viscous properties were fabricated: transparent TPU and PTFE film, frosted TPU film and three types of Ecoflex foam films with varying adhesion levels. The foaming microsphere doping concentrations in these Ecoflex films were 15 wt%, 10 wt%, and 5 wt%, respectively. By adjusting the doping concentration of the foaming microspheres, triboelectric materials with different adhesion characteristics were prepared. Triboelectric materials with different viscosities were prepared by varying the doping concentration of foamed microspheres. As the foaming degree increases, the viscosity decreases; notably, the frosted TPU film exhibits nearly no viscosity compared to the transparent TPU film. For comparative analysis, transparent TPU and PTFE films were also tested. When the PTFE film comes into contact with the transparent TPU film, the interaction produces minimal viscous force, making it an ideal reference for comparison.

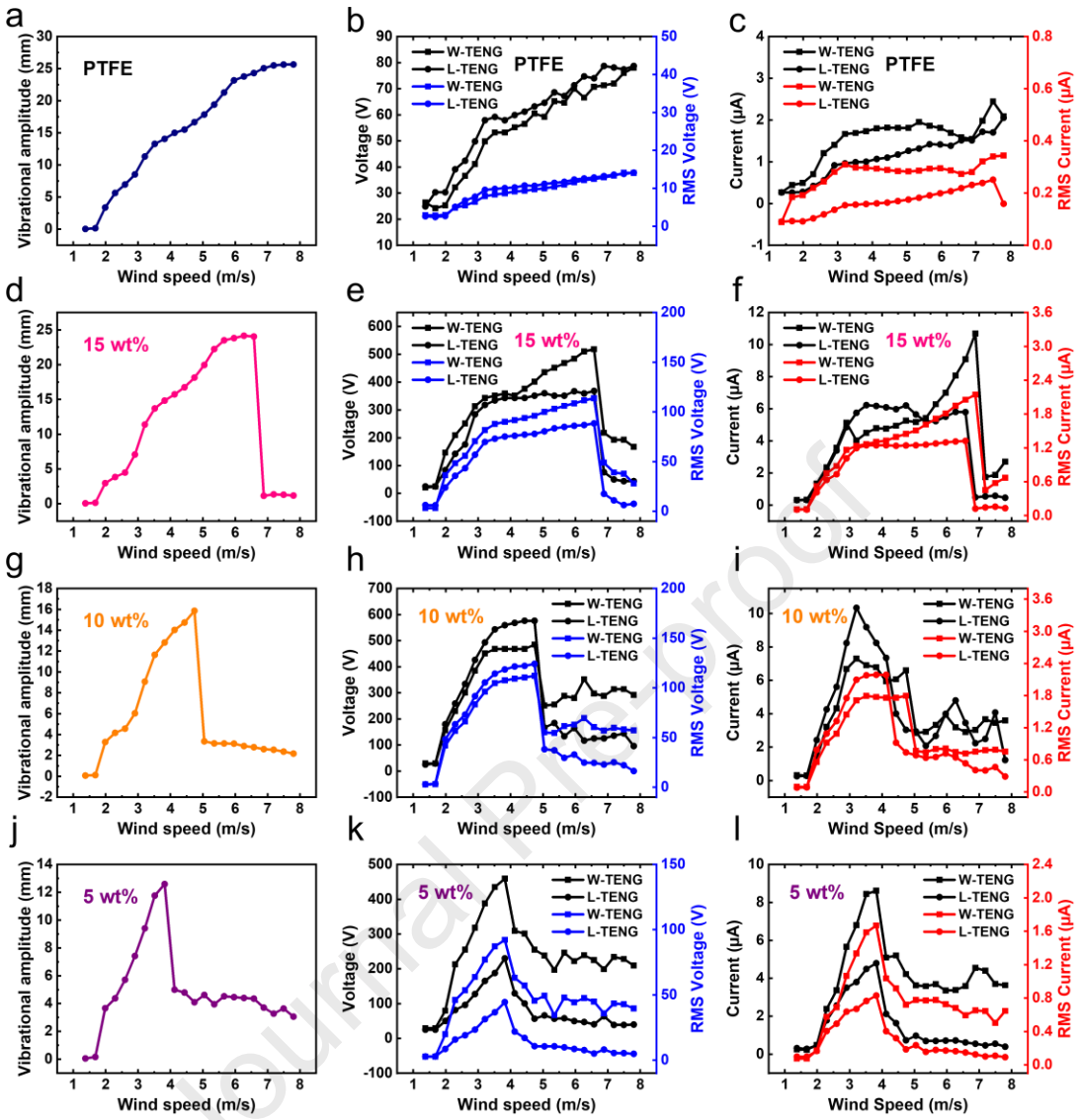

Fig.3 Influence of material viscosity on the NG-TEHG performance. (a, b, c) Vibration amplitude of the bluff body and output voltage and current of the TENG when PTFE is used as the triboelectric material. (d, e, f) Vibration amplitude of the bluff body and output voltage and current of the TENG when the 15 wt% Ecoflex foam film is used. (g, h, i) Vibration amplitude of the bluff body and output voltage and current of the TENG when the 10 wt% Ecoflex foam film is used. (j, k, l) Vibration amplitude of the bluff body and output voltage and current of the TENG when the 5 wt% Ecoflex foam film is used.

As the viscosity of the triboelectric material increases, the cutoff wind speed exhibits a decreasing trend, as shown in **Fig. 3**(a, d, g, j). The cutoff wind speed was observed at 6.58 m/s, 4.74 m/s, and 3.82 m/s, respectively. This trend is attributed to the increased difficulty in achieving separation after contact between the spring steel sheet and arc wall, leading to a mismatch between TENG operation and bluff body

vibration. When the galloping amplitude exceeds a certain threshold, the TENG undergoes maximum deformation, and the viscous force between the triboelectric materials reaches its peak. This directly disrupts the motion of the spring steel sheet, preventing the TENG from maintaining resonance with the bluff body's galloping motion. At this stage, the galloping vibration mode becomes entirely disrupted, and the fluid-structure interaction with wind is significantly weakened or lost, leading to reduced or decreased vibration. As shown in **Fig. 3**(b, c), the TENG exhibits significantly lower output performance when PTFE is used as the triboelectric material compared to when Ecoflex foam film is used. This demonstrates that the working range of the NG-TEHG can be effectively tuned by adjusting the material viscosity. When using 15 wt% Ecoflex foam film, the TENG achieves an optimal operating range of 1.98–6.58 m/s, with the maximum open-circuit voltage reaching 518 V for the W-TENG and 368 V for the L-TENG, as shown in **Fig. 3**(e, f). When using 10 wt% Ecoflex foam film, the W-TENG achieves a maximum open-circuit voltage of 576 V, an RMS voltage of 124.1 V, a maximum short-circuit current of 10.33 μA, and an RMS current of 2.18 μA. The output of TENGs is typically short and pulsed, with voltages mostly far below the peak level, making it ineffective for evaluating the energy harvesting performance. Therefore, a comprehensive and scientific performance evaluation must include both metrics. The L-TENG achieves a maximum open-circuit voltage of 485 V, an RMS voltage of 112.1 V, a maximum short-circuit current of 7.3 μA, and an RMS current of 1.79 μA. Beyond the optimal operating range of 1.98-4.74 m/s, the bluff body continues to maintain small-amplitude vibrations, allowing the TENG to remain functional. This endows the NG-TEHG with the dual advantages: 1) The NG-TEHG exhibits a broad operational bandwidth, functioning effectively at wind speeds ranging from 1.98 m/s to 4.74 m/s. 2) At wind speeds exceeding 4.74 m/s, the amplitude of the bluff body no longer increases indefinitely due to the nonlinear resistance limiting its motion. Instead, it demonstrates small-amplitude oscillations, thereby protecting the structure, as demonstrated in **Fig. 3**(h, i). When using 5 wt% Ecoflex foam film, the

TENG's optimal working range is limited to 1.98-3.822 m/s, with only small-amplitude vibrations (below 6 mm) maintained between 3.82 m/s and 7.80 m/s. Consequently, the output performance is notably lower than that achieved using 10 wt% Ecoflex foam film, as shown in **Fig. 3**(k, l). In the W-TENG, the spring steel sheet and the arc wall are subjected to an additional force induced by wind pressure, which enhances the contact force between the two triboelectric materials. As a result, the open-circuit voltage of the W-TENG is higher than that of the L-TENG. Based on the experimental results, it can be concluded that as the content of foaming microspheres gradually decreases (from 15 wt% to 5 wt%), the amplitude of the bluff body gradually decreases, and the wind speed corresponding to the maximum amplitude also reduces. Meanwhile, the maximum output voltage exhibits a trend of increasing first and then decreasing.

3.3. Output characteristics and practical applications of the NG-TEHG

Through a quantitative analysis of the three factors, i.e., the surface shape (s) of the arc wall, the initial distance (d) between the friction surfaces, and the viscosity (η) of the triboelectric material, the fundamental operating principle of the NG-TEHG was established. As shown in **Fig. 3**(g, h, i), when using 10 wt% Ecoflex foam film, the bluff body achieves a maximum galloping amplitude of 15.8 mm, and the TENG generates considerable outputs at wind speeds below 4.74 m/s. When the wind speed exceeds 4.74 m/s, the TENG continues to operate with a certain level of efficiency, sustained by the small-amplitude vibrations of the bluff body, thereby ensuring a wide working range. Therefore, the 10 wt% Ecoflex foam film and frosted TPU film were selected as the triboelectric materials for the NG-TEHG.

Additionally, to prevent collisions between the magnet and coil and to ensure that the bar magnet can move freely within the coil at high amplitudes, the distance D between the top of the bar magnet and the coil was set to 20 mm. As shown in **Fig. 4**(a), the bluff body vibration of the NG-TEHG first increases in amplitude with rising wind speed, then decreases, and eventually stabilizes at a small amplitude of approximately

4 mm once the wind speed exceeds 4.74 m/s. Under this condition, the open-circuit voltage and short-circuit current outputs from the TENG unit are shown in **Fig. 4**(b, c). It demonstrates a steadily increasing output performance in the wind speed range of 1.98–4.74 m/s. Specifically, the W-TENG reaches a maximum open-circuit voltage of 519 V (RMS voltage of 111 V), a maximum short-circuit current of 9.07 μA (RMS current of 1.87 μA). In comparison, the L-TENG achieves a maximum open-circuit voltage of 389 V (RMS voltage of 84.3 V), a maximum short-circuit current of 9.88 μA (RMS current of 1.73 μA). However, in the wind speed range of 4.74–7.80 m/s, a sudden reduction in bluff body amplitude leads to a sharp decline in the TENG output. The open-circuit voltage of the W-TENG drops to about 270 V, while that of the L-TENG falls to approximately 100 V. Due to the displacement of the bluff body in the direction of the incoming wind, the contact distance in the W-TENG decreases while that in the L-TENG increases. As a result, the W-TENG delivers a consistently higher output voltage than the L-TENG. After approximately 100,000 operating cycles, the L-TENG retains 95% of its initial output performance, while the W-TENG retains 73%, as shown in Supplementary **Fig. S5**.

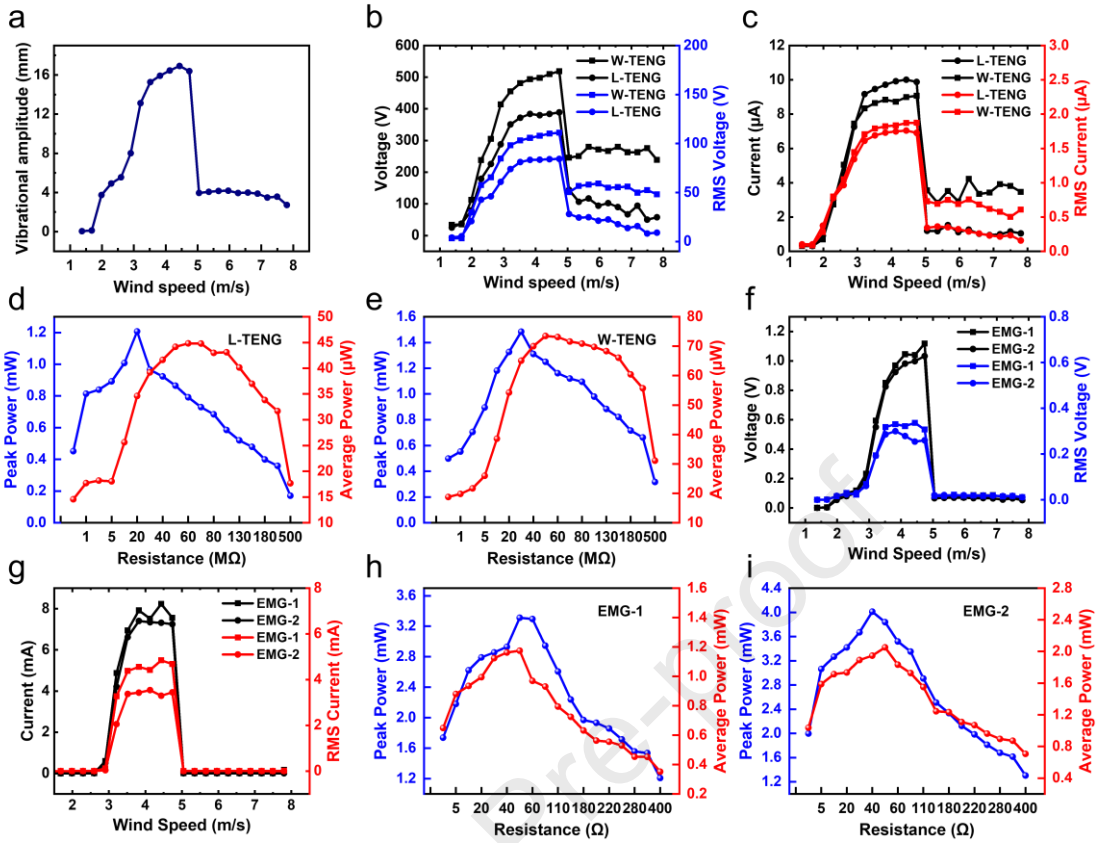

Fig.4 Output performance of the NG-TEHG. (a) Vibration amplitude of the bluff body versus the wind speed. (b, c) Open-circuit voltage and short-circuit current of the TENG versus the wind speed. (d, e) Power outputs of the L-TENG and W-TENG versus the load resistance. (f, g) Open-circuit voltage and short-circuit current of the EMG under varying wind speeds. (h, i) Power outputs of EMG-1 and EMG-2 versus the load resistance.

The power output of the TENG was evaluated at a wind speed of 4.74 m/s, and the results are offered in Supplementary **Fig. S6**. The output power of TENG was calculated as shown in **Fig. 4**(d, e). The W-TENG achieved a peak power of 1.48 mW at a load resistance of 30 MΩ, with a max RMS power of 73.48 μW at 50 MΩ. In comparison, the L-TENG attained a peak power of 1.2 mW at a load resistance of 20 MΩ, and the corresponding maximum RMS power was 44.83 μW at 60 MΩ. The reason for the above results is that the triboelectric material employed in this study is flexible Ecofoam film, which is easily deformable and covered with microsphere structures on its surface. When left and right TENGs were exposed to different pressures, the deformation of the microsphere structures varied considerably, therefore causing alterations in the internal resistance accordingly. In addition, the open-circuit voltage and short-circuit current of

the EMG as a function of wind speed are presented in **Fig. 4**(f, g). The EMG started to operate at a wind speed of 2.29 m/s, with a small amplitude of approximately 5 mm, during which the power output remained limited. In the wind speed range of 2.90–4.74 m/s, the galloping amplitude exceeded 8 mm, placing the voltage output in an optimal region. Under these conditions, EMG-1 achieved a peak-to-peak voltage of 1.11 V, an RMS voltage of 0.33 V, a peak current of 8.23 mA, and an RMS current of 4.84 mA. EMG-2 generated a peak-to-peak voltage of 1.03 V, an RMS voltage of 0.3 V, a peak current of 7.4 mA, and an RMS current of 3.54 mA. As the wind speed continued to rise, the sudden reduction in galloping amplitude caused the EMG to cease operation. The maximum power output of the EMG at a wind speed of 4.74 m/s is shown in **Fig. 4**(h, i). EMG-1 delivered a peak power of 3.31 mW and a maximum RMS power of 1.17 mW at a load resistance of 50 Ω. EMG-2 produced a peak power of 4.01 mW at a load resistance of 40 Ω and a maximum RMS power of 2.05 mW at 50 Ω. The observed results can be attributed to two primary factors: First, nonlinear perturbations between wind resistance and the springs led to inconsistencies between EMG-1 and EMG-2. Secondly, the electromagnetic induction voltage signals, which are highly sensitive to both magnet position and velocity, resulted in irregular measurements. Therefore, the optimal impedance of EMG-1 and EMG-2 differs during peak power measurement, but aligns during RMS power measurement. Overall, at a wind speed of 4.74 m/s, the NG-TEHG achieved a maximum total power output of 10 mW and an RMS power output of 3.34 mW.

In the application, the four energy harvesting units of the NG-TEHG are rectified to realize AC-to-DC conversion and then connected in parallel to power external loads, as illustrated in **Fig. 5**(a). Benefiting from the high-voltage output of the TENG units, the NG-TEHG is capable of driving high-voltage devices. As shown in **Fig. 5**(a), it can light up two display boards, i.e., one spelling “ZZU” with 32 LED bulbs and the other spelling “HKUST(GZ)” with 81 LED bulbs. Each LED operates at a forward voltage of about 1.5 V, demonstrating the system’s ability to power multi-LED configurations

effectively. **Fig. 5**(b) presents the circuit schematic of a custom-designed, self-powered IoT temperature sensing node, solely powered by the NG-TEHG. The harvested outputs are first rectified and stored in a capacitor. An energy management unit (LTC3588) then regulates the voltage to provide stable power to a BLE-enabled IoT node (NRF52832), enabling real-time temperature sensing and wireless data transmission.

The capacitor charging rate serves as a key indicator of the output performance. As shown in **Fig. 5**(c), at the wind speed of 4.74 m/s, the NG-TEHG was able to charge capacitors of 10 μF, 47 μF, 68 μF, 82 μF, 100 μF, 220 μF, and 330 μF to voltages of 13.45 V, 3.17 V, 9 V, 9.31 V, 8.74 V, 6.49 V, 4.32 V, and 2.56 V, respectively, within 60 seconds. In addition, **Fig. 5**(d, e) demonstrates the NG-TEHG's capability to power microelectronic devices at a wind speed of 4.74 m/s. Using only the TENG units, an electronic timer can be continuously powered after being charged for 60 seconds. Additionally, the NG-TEHG successfully powered the BLE-enabled IoT node (**Fig. 5**(b)), which represents a more advanced application, continuously after only 15 seconds of charging, as shown in **Fig.5**(e). The excellent performance of the NG-TEHG underscores its potential as a sustainable power solution for remote monitoring and paves the way for the development of intelligent self-powered wireless sensing systems.

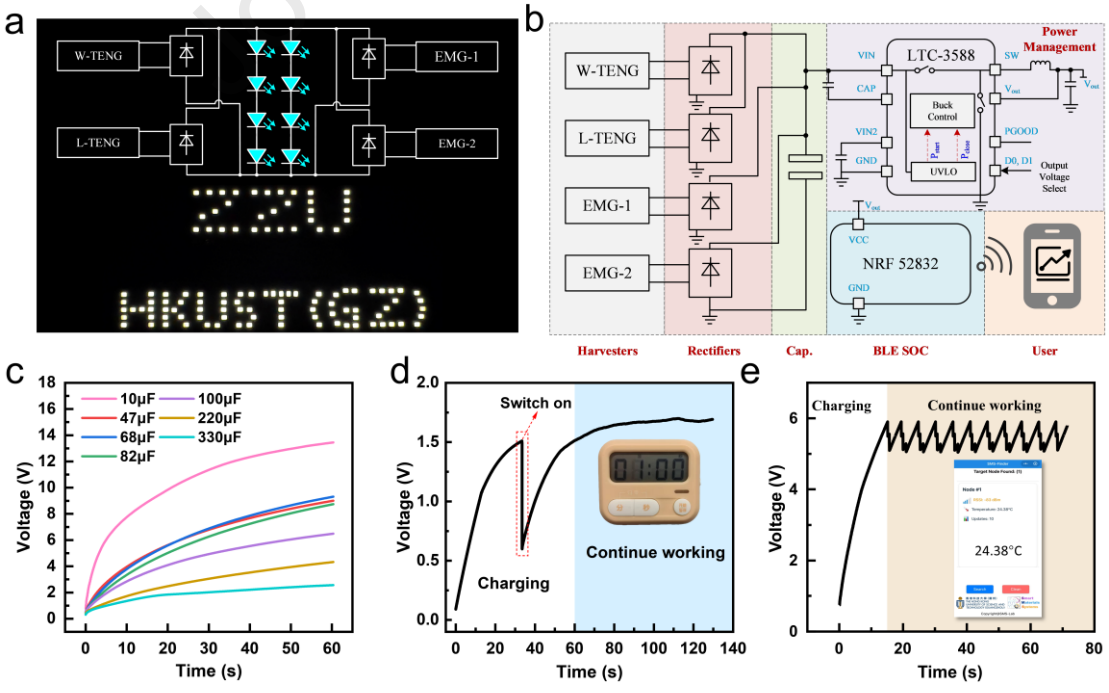

Fig.5 Self-powered applications of the NG-TEHG. (a) Demonstration of the NG-TEHG

simultaneously powering two LED display boards: “ZZU” with 32 bulbs and “HKUST(GZ)” with 81 bulbs. (b) Schematic of the self-powered IoT sensing node. Harvested energy is rectified, stored in a capacitor, and regulated by LTC3588 to power the BLE-enabled IoT node for wireless temperature sensing. (c) Testing the NG-TEHG’s capability to charge different capacitors. (d) Using the NG-TEHG to power an electronic timer. (e) Using the NG-TEHG to power a wireless temperature sensor after just 15 seconds of charging.

4. Conclusion

This work reports a novel nonlinear galloping-driven triboelectric-electromagnetic hybrid generator (NG-TEHG), designed to efficiently harvest low-speed wind energy. With a dual-mass architecture comprising bluff body-TENG elastic attachments, the system achieves tunable wind speed ranges and high electrical output through nonlinear parameter optimization. Through a comprehensive analysis of the nonlinear coupling effects between the TENG units and the galloping structure, we uncover critical insights for optimizing its energy harvesting performance. Experimental results show that the NG-TEHG could operate efficiently over a broad wind speed range of 2.29-7.80 m/s, achieving a peak power output of 10 mW and an RMS power of 3.34 mW at 4.74 m/s. At a wind speed of 4.74 m/s, the open-circuit voltage of the W-TENG unit reaches a maximum of 519 V, and that of the L-TENG unit reaches 389 V, delivering a peak power of 10 mW and an average power of 3.34 mW. These values represent improvements of 2.14 times and 18.55 times, respectively, compared to a conventional TENG device. This level of power output supports continuous operation of a wireless temperature sensor, demonstrating the system’s potential as a reliable and sustainable power source for self-powered devices. In general, the NG-TEHG presents a significant step forward in the development of self-powered systems, paving the way for more efficient and versatile energy harvesters in low-speed wind environments.

Experimental section

Design sources of three different surface-shaped arc walls

As shown in Supplementary **Fig. S2**, when the surface of the arc wall fits perfectly

with the spring steel sheet's deformation, the contact area of the TENG is maximized, leading to the strongest nonlinear effects on the bluff body of the NG-TEHG. However, the impact of these effects on the bluff body vibration remains uncertain. To investigate the influences of different surface shapes, dynamic deformation images of the spring steel sheet, captured by a Megapixel Network Surface Array Camera, were analyzed frame by frame. Distance markers were applied along both the X and Y axes on the images, and the distance data were fitted to determine the cross-sectional shape of the deformed spring steel sheet. This analysis led to the design of two symmetric profiles, Symmetry-1 and Symmetry-2, that correspond to the vibration of the spring steel sheet. For comparison, an asymmetric curved surface, resembling the shape of a water droplet (semi-droplet-shaped surface), was also designed. This surface shape induces a lateral force F_τ during contact, which can leverage the material's viscosity characteristics to enhance the output performance, though it may result in increased material wear.

Preparation process of the Ecoflex foam film

The preparation of the Ecoflex foam film begins by weighing equal amounts of Ecoflex^{TM}00-30 A and Ecoflex^{TM}00-30 B solutions (Smooth-on, America). Subsequently, the material is doped by adding thermally expandable microspheres (120DU25, Polychem, America) with different mass fractions into the Ecoflex mixed solution. The mixture is stirred thoroughly to ensure uniform dispersion of the microspheres throughout the solution. During the curing process, it is crucial to ensure adequate degassing for optimal foaming. To remove any small bubbles formed during stirring, the Ecoflex-microsphere mixture undergoes vacuum treatment. The degassed solution is then evenly applied to a pre-treated Polyvinyl chloride (PVC) sheet, followed by pressing with a glass plate to ensure a uniform film thickness. After curing at room temperature for 5 hours, the film is placed in a vacuum oven at 100°C for 30 minutes to complete the whole process, resulting in an Ecoflex foam film with a protruding microsphere surface structure.

Fabrication of the NG-TEHG

The bluff body, the top plate of the TENG, and the base were fabricated using 3D printing with PLA material. The bluff body springs, TENG springs, spring steel sheets, TPU films, PTFE films, magnets, and coils were all commercially sourced. The TENG and the bluff body were mounted on an aluminum profile frame, and the TENG was fully enclosed in an acrylic shell.

Resources availability

Materials availability

***

Data and code availability

***

Supporting Information

Author contributions

***

Acknowledgments

***

Conflict of interest

The authors declare that they have no known competing financial interests or personal relationships that could have appeared to influence the work reported in this paper.

References:

1 Cheng, T. H. *et al.* Triboelectric nanogenerators. *Nature Reviews Methods Primers* **3** (2023). https://doi.org/10.1038/s43586-023-00220-3

2 Yang Y. *et al.* Contact-sliding-separation mode triboelectric nanogenerator. *Energy & Environmental Science* **16** (2023). https://doi.org/10.1039/D3EE01290E

3 Wang, J. L. *et al.* Improving mechanical energy harvesters without complex fabrication using

origami/kirigami. *Device* **2** (2024). https://doi.org/10.1016/j.device.2024.100548

4 Yang, K. *et al*. Magnet-induced monostable nonlinearity for improving the VIV-galloping-coupled wind energy harvesting using combined cross-sectioned bluff body. *Smart Materials and Structures* **29** (2020). https://doi.org/10.1088/1361-665X/ab874c

5 Wu, M. W. *et al.* Recent advances in nanogenerators driven by flow-induced vibrations for harvesting energy. *Materials Today Energy* **41** (2024). https://doi.org/10.1016/j.mtener.2024.101529

6 Tian, H. G. *et al*. Enhanced airfoil-based flutter piezoelectric energy harvester via coupling magnetic force. *Applied Energy* **340** (2023). https://doi.org/10.1016/j.apenergy.2023.120979

7 Wang, J. L. *et al.* Energy concentration pipe based on passive jet control for enhancing flow induced vibration energy harvesting. *Energy Conversion and Management* **319** (2024). https://doi.org/10.1016/j.enconman.2024.118948

8 Xia, B. *et al*. Enhanced performance of piezoelectric energy harvester by installing symmetrical flexible splitter plates. *Mechanical Systems and Signal Processing* **225** (2025). https://doi.org/10.1016/j.ymssp.2024.112257

9 Ma, X. Q. *et al*. A review of flow-induced vibration energy harvesters. *Energy Conversion and Management* **254** (2022). https://doi.org/10.1016/j.enconman.2022.115223

10 Li H T. *et al.* Theoretical and experimental study of a bi-stable piezoelectric energy harvester under hybrid galloping and band-limited random excitations. *Applied Mathematics and Mechanics-English Edition* **45** (2024). https://doi.org/10.1007/s10483-024-3098-5

11 Zheng T. *et al.* Improving the wind energy harvesting performance with double upstream fractal bluff bodies. *Renewable Energy* **239** (2025). https://doi.org/10.1016/j.renene.2024.122070

12 Bae, J. *et al.* Flutter-driven triboelectrification for harvesting wind energy. *Nature Communications* **5** (2014). https://doi.org/10.1038/ncomms5929

13 Zhao, Z. F. *et al.* Freestanding Flag-Type Triboelectric Nanogenerator for Harvesting High-Altitude Wind Energy from Arbitrary Directions. *Acs Nano* **10**, 1780-1787 (2016). https://doi.org/10.1021/acsnano.5b07157

14 Yu, X. K. *et al.* Moisture Resistant and Stable Wireless Wind Speed Sensing System Based on Triboelectric Nanogenerator with Charge-Excitation Strategy. *Advanced Functional Materials* **32** (2022). https://doi.org/10.1002/adfm.202207498

15 Son, J. H. *et al.* Wind-Driven Bidirectional Fluttering Triboelectric Nanogenerator Via Dual Flagpole and Slot Structure Design. *Advanced Materials Technologies* **8** (2023). https://doi.org/10.1002/admt.202200453

16 Yue, O. Y. *et al.* A bladeless wind-tunnel generator based on a flutter-driven triboelectric nanogenerator with on-demand micro-structuring. *Nano Energy* **128** (2024). https://doi.org/10.1016/j.nanoen.2024.109886

17 Han, Y. *et al.* Enhance vortices vibration with Y-type bluff body to decrease arousing wind speed and extend range for flag triboelectric energy harvester. *Nano Energy* **119** (2024). https://doi.org/10.1016/j.nanoen.2023.109063

18 Yuan, S. L. *et al.* Scavenging breeze wind energy (1-8.1 ms^{-1}) by minimalist triboelectric nanogenerator based on the wake galloping phenomenon*. *Nano Energy* **100** (2022).

https://doi.org/10.1016/j.nanoen.2022.107465

19 Dong, L. W. *et al.* Metasurface-enhanced multifunctional flag nanogenerator for efficient wind energy harvesting and environmental sensing. *Nano Energy* **124** (2024). https://doi.org/10.1016/j.nanoen.2024.109508

20 Thantharate, P. *et al.* GREENSKY: A fair energy-aware optimization model for UAVs in next-generation wireless networks. *Green Energy and Intelligent Transportation* **3** (2024). https://doi.org/10.1016/j.geits.2023.100130

21 Thulasingam, M. *et al.* Radial distribution systems performance enhancement through RE (Renewable Energy) integration and comprehensive contingency ranking analysis.*Green Energy and Intelligent Transportation* **4** (2025). https://doi.org/10.1016/j.geits.2024.100245

22 Lv, Y. F. *et al.* A comprehensive review of nonlinear oscillators in hydrokinetic energy harnessing using flow-induced vibrations. *Renewable & Sustainable Energy Reviews* **150** (2021). https://doi.org/10.1016/j.rser.2021.111388

23 Zeng, Q. X. *et al.* A high-efficient breeze energy harvester utilizing a full-packaged triboelectric nanogenerator based on flow-induced vibration. *Nano Energy* **70** (2020). https://doi.org/10.1016/j.nanoen.2020.104524

24 Guo, X. *et al.* Enhance Charge Transfer and Reduce Internal Resistance for Triboelectric Nanogenerator via Switching Charge Shuttling. *Advanced Energy Materials* (2024). https://doi.org/10.1002/aenm.202405116

25 Han, P. *et al.* Vortex-induced vibration forever even with high structural damping. *Journal of Fluid Mechanics* **962** (2023). https://doi.org/10.1017/jfm.2023.268

26 Kim, J. S. *et al.* Collectively Exhaustive Hybrid Triboelectric Nanogenerator Based on Flow-Induced Impacting-Sliding Cylinder for Ocean Energy Harvesting. *Advanced Energy Materials* **12** (2022). https://doi.org/10.1002/aenm.202103076

27 Zhang, L. B. *et al.* Galloping triboelectric nanogenerator for energy harvesting under low wind speed. *Nano Energy* **70** (2020). https://doi.org/10.1016/j.nanoen.2020.104477

28 Wang, J. L. *et al.* TENG using nonlinear coupling galloping phenomenon for harvesting wind energy. *Nano Energy* **133** (2025). https://doi.org/10.1016/j.nanoen.2024.110471

29 Zhang, L. B. *et al.* Vortex-induced vibration triboelectric nanogenerator for low speed wind energy harvesting. *Nano Energy* **95** (2022). https://doi.org/10.1016/j.nanoen.2022.107029

30 Nishi, Y. Power extraction from vortex-induced vibration of dual mass system. *Journal of Sound and Vibration* **332**, 199-212 (2013). https://doi.org/10.1016/j.jsv.2012.08.018

31 Nishi, Y. *et al.* Experimental energy harvesting from fluid flow by using two vibrating masses. *Journal of Sound and Vibration* **394**, 321-332 (2017). https://doi.org/10.1016/j.jsv.2017.01.037

32 Liu, J. L. *et al.* Marine energy harvesting from tidal currents and offshore winds: A 2-DOF system based on flow-induced vibrations. *Nano Energy* **114** (2023). https://doi.org/10.1016/j.nanoen.2023.108664

33 Liu J. B. *et al.* A joint model of infrastructure planning and smart charging strategies for shared electric vehicles. *Green Energy and Intelligent Transportation* **3** (2024). https://doi.org/10.1016/j.geits.2024.100168

34 Yang Y. *et al.* Material's selection rules for high performance triboelectric nanogenerators. *Materials Today* **64** (2023). https://doi.org/10.1016/j.mattod.2023.03.008

35 He, L. X. *et al.* Dynamic interfacial electrostatic energy harvesting via a single wire. *Science Advances* **10** (2024). https://doi.org/10.1126/sciadv.ado5362

36 Yang Y. *et al.* Substantially boosting performance of triboelectric nanogenerators via a triboelectrification enhancement effect. *Joule* **8** (2024) https://doi.org/10.1016/j.joule.2024.04.013

37 Sun, H. *et al.* Hydrokinetic power conversion using Flow Induced Vibrations with nonlinear (adaptive piecewise-linear) springs. *Energy* **143**, 1085-1106 (2018). https://doi.org/10.1016/j.energy.2017.10.140

38 Zhang, B. S. *et al.* Vortex-Induced Vibration (VIV) hydrokinetic energy harvesting based on nonlinear damping. *Renewable Energy* **195**, 1050-1063 (2022). https://doi.org/10.1016/j.renene.2022.06.102

Highlights:

1. A nonlinear galloping-driven triboelectric–electromagnetic hybrid generator (NG-TEHG) is developed for efficient low-speed wind energy harvesting.
2. Nonlinear structural and material tuning enables wideband operation (2.29–7.80 m/s) with a peak output of 10 mW.
3. The NG-TEHG powers LEDs and a wireless IoT sensor, demonstrating practical self-powered applications.

Declaration of interests

☒ The authors declare that they have no known competing financial interests or personal relationships that could have appeared to influence the work reported in this paper.

☐ The authors declare the following financial interests/personal relationships which may be considered as potential competing interests: